J|A|C|S
COMMUNICATIONS

Published on Web 09/06/2006

Radial-Position-Controlled Doping in CdS/ZnS Core/Shell Nanocrystals

Yongan Yang, Ou Chen, Alexander Angerhofer, and Y. Charles Cao*

Department of Chemistry, University of Florida, Gainesville, Florida 32611

Received July 6, 2006; E-mail: cao@chem.ufl.edu.

The ability to precisely control the doping of semiconductor nanocrystals can create an opportunity for producing functional materials with new properties, which are of importance to applications such as biomedical diagnosis, solar cells, and spintronics.[1−4] This opportunity has stimulated research efforts to develop synthetic methods to incorporate dopants into a variety of colloidal semiconductor nanocrystals.[2−5] It has been found that nanocrystals with dopants inside their crystal lattice can exhibit different properties from those with dopants on their surface.[2−5] However, experimental data is still lacking on the fundamental question of whether different dopant positions inside nanocrystals can affect physical properties of doped nanocrystals. Herein, we report a colloidal synthesis of high-quality CdS/ZnS core/shell nanocrystals with radial-position-controlled Mn dopants. We demonstrate that the room-temperature (rt) photoluminescence (PL) quantum yield (QY) of Mn dopants strongly depends on their radial positions inside the host core/shell nanocrystals.

Our approach to the radial-position-controlled doping of semiconductor nanocrystals is based on a three-step colloidal synthesis: (1) synthesis of "starting host particles," (2) Mn-dopant growth, and (3) host−shell growth (Figure 1a−c). The syntheses in the first and third steps are carried out by a modification of the literature methods.[6,7] The diameter of the starting host particles and the thickness of host shells determine the radial positions of Mn dopants inside the host core/shell nanocrystals. In the second step, Mn-doping is achieved by the growth of partial MnS shells onto the starting host particles. Mn-doping levels (i.e., concentration of the dopants) of the nanocrystals are controlled in this step in direct proportion to the amount of MnS-growth precursors added (e.g., $Mn(Ac)_2$ and S).[7] Elemental analysis of as-prepared nanocrystals using inductively coupled plasma atomic emission spectroscopy (ICP) shows that only around 30% of the Mn in the precursors can grow onto the starting host particles. To achieve a more precise control of the Mn position inside the nanocrystals, a separation is carried out to remove the unreacted Mn-species from the growth solution before host−shell growth in the third step.

The major difficulty in the second step lies in Ostwald ripening of the nanocrystals, which can lead to a broadening of their size distributions. When the starting host particles are pure CdS (i.e., Ia and Ib in Figure 1), the Mn-dopant growth led to significant ripening of nanocrystals at high temperatures (e.g., 280 °C), and the size distribution of nanocrystals quickly broadened.[7] To minimize Ostwald ripening of the nanocrystals, we chose an active single molecular precursor (i.e., $Mn(S_2CNEt_2)_2$) for low-temperature dopant growth (e.g., 220 °C). In contrast to CdS nanocrystals, when the starting host particles are CdS/ZnS core/shell particles (Ic in Figure 1), no substantial ripening occurred during Mn-dopant growth, even at 280 °C.[7] This chemical nature allows the use of less-active precursors (i.e., $Mn(Ac)_2$ and S) for Mn-dopant growth on these core/shell nanocrystals. These less-active precursors are exchangeable with the active precursor during the dopant growth on CdS/ZnS core/shell nanocrystals at 280 °C.

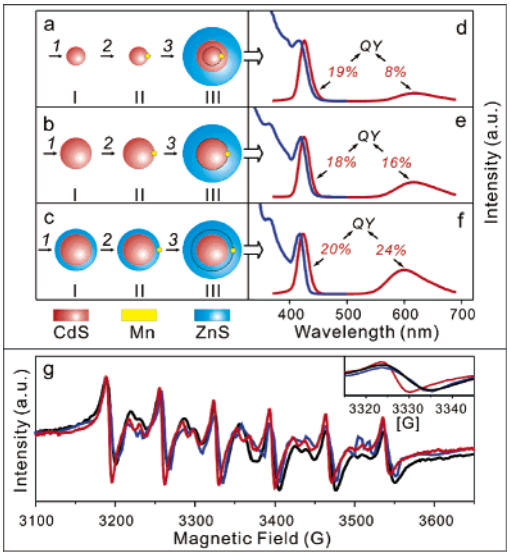

Figure 1. A scheme of Mn-doped CdS/ZnS core/shell nanocrystals with different Mn positions: (a) inside the CdS core, (b) at the core/shell interface, and (c) in ZnS shell. The final core/shell particles (i.e., IIIa, IIIb, and IIIc) have CdS core diameter of 3.8 nm (with a standard deviation σ of ~8%) and ZnS shell thickness of 1.5 nm (σ ~8%). Also shown are the PL spectra (in red) and PL excitation spectra (in blue, λ_{em} = 600 nm) of the core/shell nanocrystals: (d) IIIa, (e) IIIb, and (f) IIIc. The corresponding EPR spectra (taken at 9.5 GHz and 6 K) are shown in panel g as the black (IIIa), blue (IIIb), and red (IIIc) lines. Inset is a zoom-in plot of the third peak of these EPR spectra.

To explore the effects of position-controlled Mn doping, we synthesized three types of CdS/ZnS core/shell nanocrystals with Mn dopant at different positions: inside the CdS core (IIIa), at the core/shell interface (IIIb), and in the ZnS shell (IIIc, Figure 1). The data from transmission electron microscope (TEM) and IPC show that these three types of Mn-doped core/shell nanocrystals have a nearly identical CdS-core size, ZnS-shell thickness, and Mn-doping level (0.10%, ~4 Mn atoms per particle). These Mn-doped nanocrystals exhibit two PL bands: the blue band is assigned to the emission from exciton recombination in the core/shell nanocrystals, and the red band is assigned to the emission from Mn dopants ($^4T_1$ to $^6A_1$, Figure 1d−f).[3,4] The PL excitation spectra of these CdS/ZnS nanocrystals indicate that energy transfer from the exciton in the nanocrystals to the Mn dopants gives rise to the red emission.[3] In addition, these nanocrystals exhibit a nearly identical absorption peak position for their first exciton band. This result is consistent with TEM measurements demonstrating that the CdS core size is nearly identical for these Mn-doped core/shell nanocrystals.

Importantly, these Mn-doped nanocrystals exhibit dopant-position-dependent optical properties (Figure 1d−f). The QY of the blue-exciton emission is similar for these nanocrystals, but the QY of the Mn emission is substantially different for the nanocrystals with Mn dopants inside a CdS core (8%), at the core/shell interface (16%), and in the ZnS shell (24%). These results indicate that the

10.1021/ja064818h CCC: $33.50

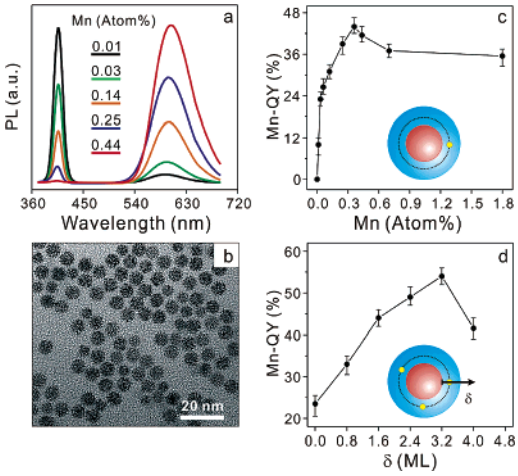

Figure 2. (a) Normalized PL spectra of Mn-doped CdS/ZnS core/shell nanocrystals with different doping levels. These core/shell nanocrystals have a CdS core diameter of 3.1 nm (σ ~6%), ZnS-shell thickness is 1.5 nm (~4.8 ML), and the Mn dopants are located at 1.6 ML in the shell. Shown also are (panel b) a typical TEM image of the Mn-doped core/shell nanocrystals, (panel c) a plot of Mn QY as a function of doping level for these nanocrystals, and (panel d) a plot of Mn QY as a function of Mn position (δ) in the ZnS shell of the core/shell nanocrystals with a doping level of 0.36%.

nonradiative decay of the Mn excited state ($^4T_1$)—not the overlap between the Mn and exciton wave functions (i.e., energy transfer from the exciton to the Mn)—plays the dominant role in controlling the Mn-emission QY. Therefore, the position-dependent Mn-emission QY would be caused by the following two factors: (1) the Mn−Mn interactions inside a doped core/shell nanocrystal, and (2) the local crystal-field strain on the Mn dopants.

The Mn positions inside the core/shell nanocrystals were identified using electron paramagnetic resonance (EPR) spectroscopy. These three types of core/shell nanocrystals exhibit a six-line spectrum with a similar hyperfine coupling constant of about 69.7 G (Figure 1g). Such a hyperfine coupling constant indicates that the Mn dopants are at cubic CdS or ZnS lattice sites, and thus the dopants are indeed located inside the core/shell nanocrystals.[8a] This result is consistent with X-ray powder diffraction (XRD) measurements that these core/shell nanocrystals have a zinc blende (i.e., cubic) crystal structure.[7] In addition, the line-width of the EPR peaks is different for the nanocrystals with Mn dopants in the CdS core (12 G), at the core/shell interface (12 G), and in the ZnS shell (7.4 G, inset of Figure 1g). The narrower EPR-peak line-width indicates weaker Mn−Mn interactions and less local strain on the Mn dopants in the ZnS shell.[8b] Both effects can lead to less nonradiative decay of the Mn excited state, and therefore, a higher Mn-emission QY for the core/shell particles with Mn in the shell. It is consistent with the results from optical measurements (Figure 1d−f). Taken together, the results from both optical and EPR measurements suggest that radial-position-controlled Mn-doping of CdS/ZnS nanocrystals is achieved by the three-step synthesis.

The three-step synthesis allows a systematic study of the effects of Mn-doping level of CdS/ZnS core/shell nanocrystals (Figure 2a−c). Nine types of core/shell nanocrystals were synthesized with Mn-doping levels from 0.013% to 1.8%. These nanocrystals have a 3.1 nm CdS core coated with a ZnS shell of 4.8 monolayers (ML), and Mn dopants are at 1.6 ML in the shell. The Mn-doping levels were determined by ICP measurements. A TEM image of a typical nanocrystal sample shows that the Mn-doped core/shell nanocrystals are nearly monodispersed with a standard deviation of 6% (Figure 2b). With the increase of the Mn-doping level, the QY of the Mn emission increases, while the QY of blue-exciton emission decreases (Figure 2a). The exciton emission is totally quenched when the doping level reaches 0.44%. This result further demonstrates that Mn-emission originates from the energy transfer from exciton of the core/shell particles to the Mn.[3,4] In addition, the QY of Mn emission reaches a maximum of around 44% when the doping level is 0.36% (Figure 2c). With a further increase of the Mn-doping level, the QY of the Mn emission decreases. This further increase in Mn-doping level could cause stronger Mn−Mn interactions and/or create greater crystal-field strain in ZnS shells. Both cases can increase nonradiative decay of the Mn excited state, and thus lead to a decreased Mn-emission QY.

To produce nanocrystals with a higher Mn-emission QY, we further investigated the effects of detailed Mn positions inside the ZnS shell of the core/shell nanocrystals. Keeping the core size and shell thickness unchanged (as those in the study of doping-level effects, Figure 3c) we chose a Mn-doping level of 0.36% for this study. Six types of nanocrystals were synthesized with Mn position (δ) varying from 0 to 4.0 ML inside the ZnS shell (Figure 2d). Surprisingly, the QY of the Mn emission strongly depends on the Mn position. The Mn-emission QY increases with the increase of δ. A maximum QY up to 56% is achieved at δ of 3.2 ML, and then the QY decreases with the further increase of δ (Figure 2d). This position-dependent Mn emission could be, in part, caused by the inhomogeneity of local crystal-field strain inside the ZnS shell caused by the 7% lattice mismatch between the CdS and ZnS crystal lattice.[6]

In conclusion, we have developed a new doping approach, using a three-step synthesis to produce high-quality Mn-doped CdS/ZnS core/shell nanocrystals. This approach allows the precise control of Mn radial position and doping level in core/shell nanocrystals. Second, we have shown the first example in which optical properties of Mn-doped nanocrystals strongly depend on Mn radial positions inside the nanocrystal. Third, we have synthesized nanocrystals with a rt Mn-emission QY of 56%, which is nearly twice as high as that of the best Mn-doped nanocrystals reported previously.[2−5] Such a high QY is very important to applications such as nanocrystal-based biomedical sensing.[1]

Acknowledgment. This work was supported by the University of Florida, and the NHMFL IHRP (A.A.).

Supporting Information Available: Detailed synthetic procedure, absorption spectra of Mn-doped CdS nanocrystals, and XRD data. This material is available free of charge via the Internet at http://pubs.acs.org.

References

(1) (a) Alivisatos, A. P. *Nat. Biotechnol.* **2004**, *22*, 47. (b) Han, M.; Gao, X.; Su, J. Z.; Nie, S. *Nat. Biotechnol.* **2001**, *19*, 631.
(2) Shim, M.; Wang, C.; Norris, D. J.; Guyot-Sionnest, P. *MRS Bull.* **2001**, *26*, 1005.
(3) Erwin, S. C.; Zu, L.; Haftel, M. I.; Efros, A. L.; Kennedy, T. A.; Norris, D. J. *Nature* **2005**, *436*, 91.
(4) Pradhan, N.; Goorskey, D.; Thessing, J.; Peng, X. *J. Am. Chem. Soc.* **2005**, *127*, 17586.
(5) (a) Norris, D. J.; Yao, N.; Charnock, F. T.; Kennedy, T. A. *Nano Lett.* **2001**, *1*, 3. (b) Yang, H.; Holloway, P. H. *Appl. Phys. Lett.* **2003**, *82*, 1965. (c) Ji, T.; Jian, W.-B.; Fang, J. *J. Am. Chem. Soc.* **2003**, *125*, 8448. (d) Stowell, C. A.; Wiacek, R. J.; Saunders, A. E.; Korgel, B. A. *Nano. Lett.* **2003**, *3*, 1441. (e) Somaskandan, K.; Tsoi, G. M.; Wenger, L. E.; Brock, S. L. *Chem. Mater.* **2005**, *17*, 1190. (f) Raola, O. E.; Strouse, G. F. *Nano Lett.* **2002**, *2*, 1443. (g) Schwartz, D. A.; Norberg, N. S.; Nguyen, Q. P.; Parker, J. M.; Gamelin, D. R. *J. Am. Chem. Soc.* **2003**, *125*, 13205. (h) Bryan, J. D.; Gamelin, D. R. *Prog. Inorg. Chem.* **2005**, *54*, 47. (i) Yang, H.; Santra, S.; Holloway, P. H. *J. Nanosci. Nanotechnol.* **2005**, *5*, 1364.
(6) (a) Cao, Y.; Banin, U. *J. Am. Chem. Soc.* **2000**, *122*, 9692. (b) Xie, R.; Kolb, U.; Basche, T.; Mews, A. *J. Am. Chem. Soc.* **2005**, *127*, 7480.
(7) Supporting Information.
(8) (a) Lifshitz, E.; Francis, A. H. *J. Phys. Chem.* **1982**, *86*, 4714. (b) Kremer, R. E.; Furdyna, J. K. *Phys. Rev. B* **1985**, *31*, 1.

JA064818H